*Science Archives* (2022) Vol. 3 (4), 289-300

SCIENCE ARCHIVES

*Science Archives (ISSN:2582-6697)*

**Journal homepage: www.sciencearchives.org**

https://doi.org/10.47587/SA.2022.3408

Research Article

# Finding antagonist for the VP24 protein of the Ebola virus to treat infections using molecular docking and molecular dynamics studies

**Diptendu Sarkar ✉ and Sk Murtaj Ahamed**

*Department of Microbiology, Ramakrishna Mission Vidyamandira, Belur Math, Howrah-711202, West Bengal, India*

Received: Oct 8, 2022/ Revised: Nov 26, 2022/ Accepted: Nov 27, 2022

(✉) Corresponding Author: diptendu81@gmail.com

**Abstract**

Among all known viruses, Ebola has the unfortunate distinction of having some of the highest case-fatality rates. It is critical that new antivirals be developed to fight Ebola virus infections. A simulated screening of nearly 20 compounds against the revised protein structure of Ebola as represented by the GP24 model resulted in the selection of one molecule (CID 3851453) that may one day be used as an antiviral drug for the Ebola virus. It was found that binding energy was -7.4 Kcal/mol. The physiological and bioactivity parameters were correctly predicted together with ADMET. The 50 ns molecular dynamics simulation results' RMSD, RMSF, and Rg values showed that the proposed compound was well equilibrated and, as a result, stable in the protein-ligand complex. The substantial binding affinities of this chemical (CID 3851453) to the receptor cavity were consistent with the findings of the docking studies. Additionally, it is expected that the identified inhibitor (CID 3851453) will serve as a more advantageous starting point for future experimental studies in the hunt for antiviral medications.

**Keywords:** Ebola virus, GP24, Docking, RMSD, RMSF, Rg values

## Introduction

Ebola is indeed a viral hemorrhagic fever that affects humans and certain other mammals and is brought on by ebolaviruses. It is additionally referred to as Ebola virus disease (EVD) as well as Ebola hemorrhagic fever (EHF) (Anders et al., 1993; Antal et al., 1991). Typically, fever, sore throat, headaches, and muscle discomfort are the initial signs of an infection. Immediate interaction with body fluids, including such blood from infected individuals or other animals, or coming into contact with objects that have already being infected with infected body fluids are indeed the two main ways that the disease spreads (Arooj et al., 2013). Single-stranded, non-infectious RNA genomes are seen in ebolaviruses. A virion is expected to connect to certain cell-surface receptors, such as C-type lectins, DC-SIGN, or integrins, to start their life cycle (Azam et al., 2013). Next, the viral envelope and cellular membranes are thought to fuse. After recovery, the Ebola virus may be able to survive for longer than three months in the semen, which could result in infections through sex (Balimane et al., 2000). Eight different types of proteins being encoded by seven different gene cluster types in the EBOV genome. NP, VP35, VP40, glycoproteins (GP), sGP1, VP30, VP24, and RNA-dependent RNA polymerase seem to be the proteins that are encoded (L). The 676-residue EBOV envelope glycoprotein (EBOV-GP) and 364-residue secretory glycoprotein (sGP1) are indeed the translational products of the synthesis of the fourth gene (Beaulieu et al., 1999; Beeching et al., 2014). By preventing the virus' entrance within host cells, EBOV-GP serves as an intermediary that gives us such a feasible vaccine desired location. Furin breaks down EBOV-GP during post-translational treatment to produce the disulfide-linked GP1 and GP2 subunits (Benet et al., 2002). Like all other filoviruses, EBOV replicates effectively in a wide variety of cells, generating significant quantities of virus in monocytes, macrophages, dendritic cells, as well as liver cells, fibroblasts, and adrenal gland cells (Bissantz et al., 2000; De Oliveira et al., 2018). High levels of inflammatory chemical signals are released by viral replication, which results in a pathogenic condition.

As of now, there is no proven medication or vaccination to prevent the Ebola virus (Desai, 2016). Therefore, computational techniques and bioinformatics methodologies are helpful in the search for potential anti-Ebola medication candidates. Using the EBOV pseudo type virus, a high-throughput screen (HTS) of small-molecule compound libraries resulted in the discovery of a benzodiazepine derivative (compound 7, name 9-Ethyladanine). One of the most cutting-edge research fields, computer-aided drug design and development (CADDD), has become well-known for its dependability and economical method of finding bioactive molecules for numerous ailments (Dezani et al., 2016). Due to various potential intriguing bioactivities, natural products have been regarded as one of the most probable sources of drug candidates. Additionally, many medicines that have been offered for sale on the market have either been obtained directly from natural sources or are compounds that originate from nature (Feldmann et al., 2011; Gasteiger et al., 1980). Our primary objective in this study was to computationally model the membrane-associated protein VP24 and conduct docking studies using 20 antiviral compounds to identify a lead chemical (drug) due to its widespread production association with the ability to effectively halt replication in a wide variety of cells and constrained expression pattern of EBOV in normal tissues.

## Materials and Methods

### Modelling and refinement of protein structure

The amino acid sequence of membrane-associated protein VP24 has been obtained from Uniprot Acc NO: Q05322 (Fig 1). The membrane-associated protein VP24 model has been created by using SWISS MODEL program (https://swissmodel.expasy.org/) (Irvine et al., 1999; Sarkar et al., 2022). It is a fully automated service for homology modelling of protein structures that may be accessed using the Expasy web server or the software Deep View. A web-based integrated service devoted to modelling protein structural homology is called SWISS-MODEL. It offers instructions for creating protein homology models at various levels of complexity. There are four basic processes involved in creating a homology model: identifying the structural template(s), aligning the target sequence with the template structure(s), developing the model, and assessing the model's quality. Modern protein sequence and structural databases are integrated during these processes, which call for specialised software. Interactively repeating the aforementioned stages is possible till a satisfactory modelling outcome is obtained. Best selected model was refined by using Galaxy web server (http://galaxy.seoklab.org).

>sp|Q05322|VP24_EBOZM Membrane-associated protein VP24 OS=Zaire ebolavirus (strain Mayinga-76) OX=128952 GN=VP24 PE=1 SV=2
MAKATGRYNLISPKKDLEKGVVLSDLCNFLVSQTIQGWKVYWAGIEFDVTHKGMALLHRL
KTNDFAPAWSMTRNLFPHLFQNPNSTIESPLWALRVILAAGIQDQLIDQSLIEPLAGALG
LISDWLLTTNTNHFNMRTQRVKEQLSLKMLSLIRSNILKFINKLDALHVVNYNGLLSSIE
IGTQNHTIIITRTNMGFLVELQEPDKSAMNRMKPGPAKFSLLHESTLKAFTQGSSTRMQS
LILEFNSSLAI

**Fig. 1 Sequence of human acrosin binding protein (Uniprot Acc NO: Q05322)**

### Ligand selection and preparation for docking

Form the extensive review of literatures related to antiviral molecules, a list has prepared (Table 1). 3D structure of all antiviral drugs was downloaded from PuBChem database. The ligands have been put through an automated preparation procedure using PyRx software (Khabbaz et al., 2015; Koes 2018). There were total of 28 molecules used in this study (Table 1). The 'Ligand' option was used to rectify the torsional tree, non-polar hydrogens, charges, and atom variety once all ligands were uploaded (mol2 format) into the AutoDockTools (La Regina et al., 2011; Lee et al., 2003). With all the structure further ADME prediction were carried out by using SWISS ADME (http://www.swissadme.ch) to filter all bio active compounds based on Lipinski rule of five (Braga et al., 2016).

### Molecular docking study and simulation analysis

Molecular docking analysis was performed with target like membrane-associated best modelled protein VP24 by using PyRx virtual screening tool (Sarkar, 2021; Castillo-Garit et al., 2008). This tool used Auto Dock for docking purposes. Here first we uploaded modelled protein structure as a macromolecule and then one by one all selected bioactive compounds (ligand). The ligand energy was first reduced by software, and then it was transformed into the Auto Dock ligand format (pdbqt). Finally started docking after covering entire protein structure under grid box to screen best fitted bioactive compounds based on energy value. Approximately ten simulations were performed for each simulation, producing ten docked structures. The least energy configurations were deemed to be the highest binding conformations as a result of this. Intra-molecular associations including hydrogen bonds, van der Waals contacts, plus hydrophobic correlations with such an individual bioactive molecule have really been clearly examined using Discovery Studio software (Brehm et al., 2016; Loprinzi et al., 2011). Further by using WEBGRO -protein with ligand simulation server got the MD simulation result of best docking molecule.

**Table 1. List of drugs used for study the interaction with modelled membrane-associated VP24 protein. PubChem ID as well as their Molecular formula are also presented in the table.**

| Sl No | PubChem ID | Molecular formula |
|---|---|---|
| 1. | 3183 | $C_{11}H_{13}BrN_2O_5$ |
| 2. | 37542 | $C_8H_{12}N_4O_5$ |
| 3. | 64987 | $C_9H_{14}N_5O_4P$ |
| 4. | 91457 | $C_{15}H_{26}O$ |
| 5. | 96368 | $C_{10}H_{13}N_5O_4$ |
| 6. | 102198 | $C_{10}H_{13}N_5O_4$ |
| 7. | 254616 | $C_9H_9N_3O_9$ |
| 8. | 256623 | $C_9H_{14}N_3O_8P$ |
| 9. | 374108 | $C_{11}H_{16}N_2O_6$ |
| 10 | 416724 | $C_9H_{13}FN_2O_{12}P_2$ |
| 11 | 492405 | $C_5H_4FN_3O_2$ |
| 12 | 3851453 | $C_{17}H_{18}N_2O_7$ |
| 13 | 4369270 | $C_{23}H_{34}O_4$ |
| 14 | 5284371 | $C_{18}H_{21}NO_3$ |
| 15 | 5351180 | $C_9H_{14}ClN_3O_5$ |
| 16 | 44149862 | $C_9H_{11}BrN_2O_5$ |
| 17 | 44357643 | $C_{20}H_{13}ClN_4O_3S_2$ |
| 18 | 54678599 | $C_{10}H_{15}NO_3$ |
| 19 | 54737266 | $C_{10}H_{15}NO_3$ |
| 20 | 45038223 | $C_{21}H_{23}N_3O_4$ |
| 21 | Benztropine | $C_{21}H_{25}NO$ |

## Result and Discussion

There is a need to create a suitable medication because the lethal Ebola hemorrhagic fever brought on by EBOV is now incurable and has a high death rate (Ma et al., 2005). The VP24 surface protein, a crucial viral protein that contributes to the budding process through mediating the specialized virus-host contacts to enable the effective release of virions from the infected cells, is one promising source. Important VP24 structural and functional domains are thought to be required for effective virions and virus-like particle budding (Loprinzi et al., 2018). The Ebola VP24 protein has a variety of purposes, including being a part of the viral RNA polymerase complex, a role in viral packaging, as well as an antagonist of host interferon synthesis (Mali et al., 2019). It is therefore reasonable to combat the disease by addressing such proteins, which are crucial for proliferation and pathogenesis. Suppression of these molecules could aid in halting the pathogenesis as well as propagation of the Ebola virus (Rougeron et al., 2015).

A database of 3D protein structural models produced by the SWISS-MODEL homology modelling workflow is known as the SWISS-MODEL Repository (SMR). It gives users access to a current library of 3D protein models annotated by automated homology modelling for pertinent model species as well as experimental structural data for all UniProtKB sequences (Sarkar et al., 2022; Wadapurkar et al., 2018). Regular updates guarantee comprehensive target coverage, use of the most recent sequence and template structure databases, and full utilisation of modelling pipeline enhancements. Additionally, it enables users to evaluate the models' quality using the most recent QMEAN outcomes. If a sequence has not yet been modelled, the user may do it using the SWISS-MODEL workspace to develop models interactively (Wenthur et al., 2014). The navigation between resources for protein sequence and structure is made easier by annotating models with functional data and creating cross-links with other databases, such UniProtKB.

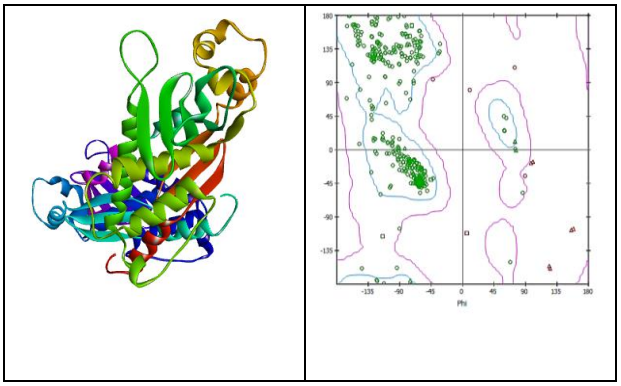

**Fig. 2 Modelled GP24 protein with Ramachandran plot**

Expect 3D protein models need to be improved in order to bring them as close to practical precision as possible in order to be used in future computational studies. The two fundamental stages of refining techniques appear to be sampling and scoring. Refining 3D models can help them resemble natural structures by altering secondary structure elements and retaping sidechains (Morris et al., 1998). On the other hand, refinement processes may unintentionally lower the quality of models. Determining whether a model has actually been improved or made worse remains a major challenge for researchers of 3D model refinement methodologies (Morris et al., 2009). Galaxy Refine uses computer simulation modelling to perform the desired architectural and recurring structure alteration. Model 2 just modifies the structure of side chain clusters, whereas models 1 through 5 make more drastic changes to loops and secondary structural systems. Utilizing the triaxial loop completion approach, model structural failures brought on by turbulence have been eliminated. Table 2 includes structure refinement data for the second modelled EBOV's GP24 protein from GalaxyRefine. Higher Rama favour suggests that the building was of higher quality. We used the PROCHECK server to analyse the Ramachandran plot.

**Table 2. Structure refinement information related to the first modelled GP24 protein of EBOV from GalaxyRefine. Higher the Rama favored indicates better the quality of the structure.**

| Model | GDT-HA | RMSD | MolProbity | Clash score | Poor rotamers | Rama favoured |
|---|---|---|---|---|---|---|
| **Initial** | 1.0000 | 0.000 | 1.554 | 3.4 | 1.0 | 93.6 |
| **MODEL 1** | 0.9751 | 0.376 | 1.695 | 8.2 | 1.0 | 96.3 |
| **MODEL 2** | 0.9661 | 0.415 | 1.496 | 8.0 | 0.5 | 97.7 |
| **MODEL 3** | 0.9774 | 0.372 | 1.644 | 9.6 | 0.5 | 97.3 |
| **MODEL 4** | 0.9762 | 0.380 | 1.686 | 10.7 | 0.0 | 97.3 |
| **MODEL 5** | 0.9762 | 0.989 | 1.810 | 10.2 | 0.5 | 95.9 |

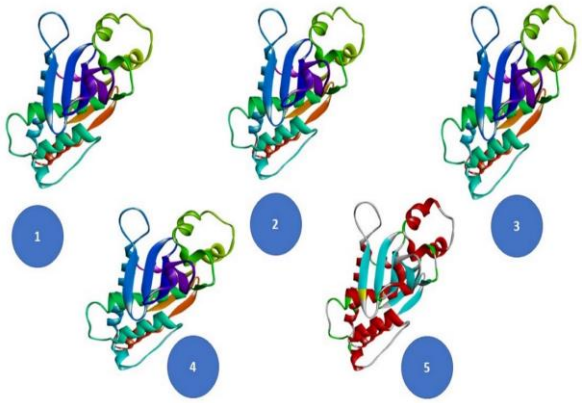


**Fig. 3 All five refined model from GalaxyRefine.**

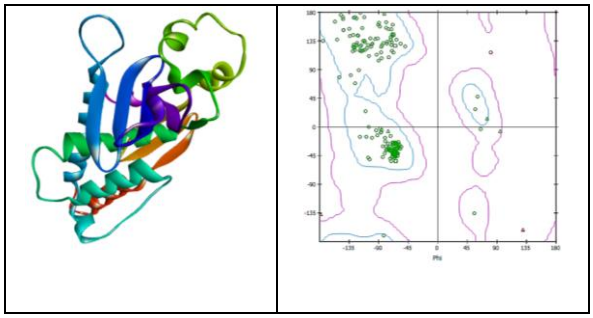

**Fig. 4 Best refined model of GP24 with Ramachandran plot. This is used for further docking study.**

The preferred orientation of one molecule to another when they should be bonded together to form a stable complex is predicted by a computer process called docking. Although it would be challenging to simulate a drug's interaction with a receptor. Hydrophobic, dispersion, or Van der Waals forces, H bonds, and electrostatic forces all play a role in intermolecular contact (Mukund et al., 2019). While hydrogen bonds and electrostatic interactions are expected to have an impact on the accuracy of the complexation, hydrophobic interactions appear to be the dominant force for binding (Nimlos et al., 2006). Modelling the intermolecular interactions in a ligand-protein molecule has proven difficult due to the wide range of possible variations and the lack of knowledge on the impact of the environment on the binding relationship. Molecular docking tries to arrange molecules into appropriate topologies in addition to connecting complementary characteristics (Oso et al., 2020; Ostroff et al., 2005). For docking research, the 3-D structure of the protein is required, and this structure is normally available and simple to obtain for any protein from the PDB database. On the other hand, the 3-D structure of the VP24 protein of EBOV is unknown. As a consequence, we examined small compounds by docking them against the modelled protein structure using computational methods to model the protein. As is common knowledge, proteins appear to be the fundamental building blocks of all living cells and play a key role in a wide range of biological processes. Every protein in our bodies has a specific function, and that function is dictated by the protein's structure (Sarkar, 2022). According to molecular modelling, conformational changes between low and high affinity states induce protein-ligand couplings (Sarkar et al., 2023). Lipid binding interactions would affect both protein structure and functioning. Characterization of couplings in protein-ligand complexes appears to be crucial for structural bioinformatics, drug development, and biological research projects (Ramalingam et al., 2011). Based on the Lipinski rule of five, or mol, ADME predictions study was performed on all drug molecules used (Table 3). 500 Daltons (g/mol) in mass, 5 H-bond donors, 10 H-bond acceptors, 5 high lipophilicity, and 40–130 molar refractive index.

**Table 3. ADME predictions analysis of all used drug molecule based on Lipinski rule of five**

| Sl. No. | PubChem ID | Molecular Weight (g/mol) | No. of Hydrogen bond donor | No. of Hydrogen bond acceptor | Log $P_{o/w}$ | Log S [ESOL] | Lipinski Rule violation |
|---|---|---|---|---|---|---|---|
| 1. | 3183 | 333.14 | 3 | 5 | 0.13 | -1.68 | 0 |
| 2. | 37542 | 244.20 | 4 | 7 | -2.05 | -0.21 | 0 |
| 3. | 64987 | 287.21 | 3 | 7 | -1.09 | -0.63 | 0 |

| | | | | | | | |
|---|---|---|---|---|---|---|---|
| 4. | 91457 | 222.37 | 1 | 1 | 3.60 | -3.51 | 0 |
| 5. | 96368 | 267.24 | 4 | 7 | -1.67 | -1.05 | 0 |
| 6. | 102198 | 267.24 | 4 | 7 | -1.67 | -1.05 | 0 |
| 7. | 254616 | 303.18 | 4 | 9 | -2.48 | -0.46 | 0 |
| 8. | 256623 | 323.20 | 5 | 9 | -2.69 | 0.24 | 1 |
| 9. | 374108 | 272.25 | 4 | 6 | -1.01 | -0.53 | 0 |
| 10. | 416724 | 422.15 | 6 | 13 | -2.81 | 1.01 | 2 |
| 11. | 492405 | 157.10 | 2 | 4 | -0.27 | -0.80 | 0 |
| 12. | 3851453 | 362.33 | 3 | 7 | 0.32 | -1.83 | 0 |
| 13. | 4369270 | 374.51 | 2 | 4 | 3.27 | -3.76 | 0 |
| 14. | 5284371 | 299.36 | 4 | 1 | 1.75 | -2.55 | 0 |
| 15. | 5351180 | 279.68 | 4 | 6 | -1.53 | -0.85 | 0 |
| 16. | 44149862 | 307.10 | 3 | 5 | -0.56 | -1.19 | 0 |
| 17. | 44357643 | 456.93 | 1 | 5 | 3.63 | -5.42 | 0 |
| 18. | 54678599 | 197.23 | 2 | 3 | 0.93 | -1.60 | 0 |
| 19. | 54737266 | 197.23 | 2 | 3 | 0.93 | -1.60 | 0 |
| 20. | 45038223 | 381.43 | 1 | 5 | 2.09 | -3.58 | 0 |
| 21. | Benztropine | 307.43 | 0 | 2 | 3.85 | -4.69 | 0 |

The goal of this research was to find specific drug with antiviral capacity, that can bind to the modelled GP24 protein, which could be employed as a therapeutic agent for EBOV in the coming days. We considered all total 20 molecules for docking along with modelled GP24 protein with energy ranges from -5.2 to -7.4 Kcal/mol (Table 4, Fig 5-25). Drug molecule having PubChem ID 3851453, showed maximum lowest binding energy i.e., -7.4 Kcal/mol. This molecule showed various interaction with modelled protein like Van deer waals, conventional hydrogen bond, covalent bond and carbon hydrogen bond. The number of hydrogen bond found was 4 in this interaction (Table 4; Fig 16). This molecule is basically Phenyl 2-[3,4-dihydroxy-5-(5-methyl-2,4-dioxopyrimidin-1-yl)oxolan-2-yl]acetate. Benztropine which is a common antiviral drug, was used as a reference molecule in this study. It showed during the interaction with modelled GP24 protein only 1 hydrogen bond along with -6.5 Kcal/mol energy (Fig 25). Therefore, it can be assumed that compound ID 3851453 has much more potency than Benztropine and can be used further for a clinical study. All other molecule's docking related information presented in Table 4 and Fig 5-25.

**Table 4. Overview of results for GP24 modelled refined protein and respective ligand binding with the Binding affinity and Number of residues in interaction as well as Number of hydrogen bond involved in the interaction.**

| Sl No | PubChem ID | Binding affinity (Kcal/mol) | Interaction residues | No. of H bonds | Bonds involved in interaction | Fig No |
|---|---|---|---|---|---|---|
| 1 | 3183 | -5.7 | Pro 204, Thr 187, Glu 180, Ile 189, Ala 208, Asn 210, Met 209, Asp 205, Gln 202, Glu 203 | 2 | Van deer waals, conventional hydrogen bond, covalent bond, Alkyl, Salt bridge | 5 |
| 2 | 37542 | -5.2 | Arg 95, Ser 123, Trp 125, Thr 128, His 186, Thr 183, Ile 188, Ala 99, Trp 92, Val 96, Leu 126, Leu 201, Thr 129, Asp 124 | 2 | Van deer waals, conventional hydrogen bond, covalent bond, Alkyl | 6 |
| 3 | 64987 | -5.8 | Ile 181, Ile 190, Ile 179, Glu 180, Thr 187, ser 178, Thr 191, Gln 202, Lys 206, Met 209, Leu 198, Val 199, Glu 200 | 1 | Van deer waals, conventional hydrogen bond, covalent bond, Pi-alkyl | 7 |
| 4 | 91457 | -6.0 | Asp 205, Ala 208, Glu 203, Gly 215, Ala 208, Pro 214, Pro 216, Asn 210, Lys 206, Met 209 | 4 | Van deer waals, carbon hydrogen bond, covalent bond, conventional hydrogen bond | 8 |
| 5 | 96368 | -5.8 | Lys 206, Ala 200, ser 207, Ile 189, His 78, Gln 202, Arg 211 | 1 | Van deer waals, conventional hydrogen bond, covalent bond, Alkyl | 9 |
| 6 | 102198 | -6.2 | Ser 207, Ala 208, Lys 213, Arg 211, Met 212, Pro 214 | 3 | Van deer waals, conventional hydrogen bond, covalent bond | 10 |
| 7 | 254616 | -5.4 | Asp 205, Ala 208, Glu 203, Gly 215, Ala 208, Pro 214, Pro 216, Asn 210, Lys 206, Met 209 | 4 | Van deer waals, conventional hydrogen bond, covalent bond, carbon | 11 |

| | | | | | | |
|---|---|---|---|---|---|---|
| | | | | | hydrogen bond | |
| 8 | 256623 | -5.6 | Glu 88, trp 92, Leu 201, Thr 86, Lys 218, Ser 85, Lys 61, Leu 79, Leu 57, Phe 80, Leu 198, ile 87, Glu 200, Val 199, Ser 220 | 2 | Van deer waals, conventional hydrogen bond, covalent bond, Pi-Pi T shaped, Pisgma, Pi-Alkyl | 12 |
| 9 | 374108 | -5.6 | Asp 205, Ala 206, Glu 203, Gly 215, Ala 208, Pro 214, Pro 216, Asn 210, Lys 206, Met 209 | 3 | Van deer waals, conventional hydrogen bond, covalent bond, carbon hydrogen bond | 13 |
| 10 | 416724 | -6.3 | Asp 205, Ala 208, Glu 203, Gly 215, Ala 208, Pro 214, Pro 216, Asn 210, Lys 206, Met 209 | 4 | Van deer waals, conventional hydrogen bond, covalent bond, | 14 |
| 11 | 492405 | -5.8 | Glu 200, Ile 189, Leu 201, Ile 190, Ala 100, Thr 183, Leu 127, Glu 180, Ile 179, Val 96, Thr 187, Ile 181 | 1 | Van deer waals, conventional hydrogen bond, covalent bond, Alkyl | 15 |
| 12 | 3851453 | -7.4 | Asp 205, Ala 208, Glu 203, Gly 215, Ala 208, Pro 214, Pro 216, Asn 210, Lys 206, Met 209 | 4 | Van deer waals, conventional hydrogen bond, covalent bond, carbon hydrogen bond | 16 |
| 13 | 4369270 | -5.8 | Asp 205, Ala 208, Glu 203, Gly 215, Ala 208, Pro 214, Pro 216, Asn 210, Lys 206, Met 209 | 4 | Van deer waals, conventional hydrogen bond, covalent bond, carbon hydrogen bond | 17 |
| 14 | 5284371 | -6.0 | Asp 205, Ala 208, Glu 203, Gly 215, Ala 208, Pro 216, Pro 214, Asn 210, Lys 206, Met 209 | 4 | Van deer waals, conventional hydrogen bond, covalent bond, carbon hydrogen bond | 18 |
| 15 | 5351180 | -5.5 | Ile 179, Val 96, Thr 187, Ile 181, Glu 200, Ile 189, Leu 201, Ile 190, Ala 100, Thr 183, Leu 127, Glu 180 | 1 | Van deer waals, conventional hydrogen bond, covalent bond, Alkyl | 19 |
| 16 | 44149862 | -5.7 | Thr 187, Leu 201, Glu 203, Lys 206, Ala 208, His 78, Met 209, Glu 200, Ile 189, Glu 203, His 186, Ala 217 | 2 | Van deer waals, conventional hydrogen bond, covalent bond, carbon hydrogen bond | 20 |
| 17 | 44357643 | -6.1 | Glu 180, Ile 189, Ala 208, Asn 210, Ser 207, Met 209, Asp 205, Gln 202, Glu 203, Pro 204, Thr 187 | 2 | Van deer waals, conventional hydrogen bond, Salt bridge, Alkyl | 21 |
| 18 | 54678599 | -5.7 | Ala 208, Lys 213, Arg 211, Met 212, Pro 214, Arg 211, Ser 207 | 3 | Van deer waals, conventional hydrogen bond, covalent bond | 22 |
| 19 | 54737266 | -5.7 | Asp 205, Ala 208, Lys 206, Glu 203, Gly 215, Ala 208, Pro 214, Pro 216, Asn 210, Lys 206, Met 209 | 4 | Van deer waals, conventional hydrogen bond, covalent bond, carbon hydrogen bond | 23 |
| 20 | 45038223 | -6.5 | Arg 95, Ser 123, Trp 125, Thr 128, His 186, Thr 183, Ile 188, Ala 99, Trp 92, Val 96, Leu 126, Leu 201, Thr 129, Asp 124 | 2 | Van deer waals, conventional hydrogen bond, covalent bond, Alkyl | 24 |
| 21 | Benztropine | -6.7 | Glu 200, Ile 189, Leu 201, Ile 190, Ala 100, Thr 183, Leu 127, Glu 180, Ile 179, Val 96, Thr 187, Ile 181 | 1 | Van deer waals, conventional hydrogen bond, covalent bond, Alkyl | 25 |

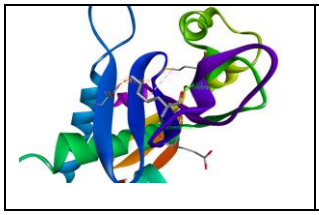
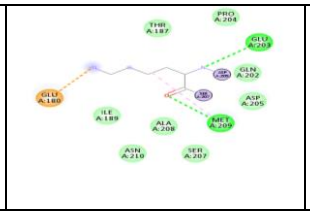
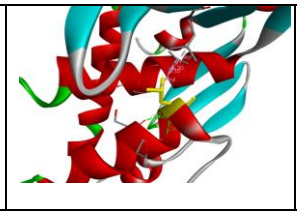
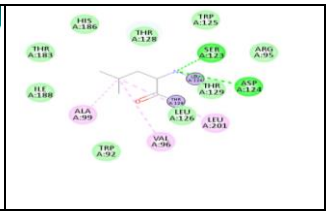

**Fig 5. 3D and 2D interaction between GP24 modelled refined protein with PubChem ID 3183**

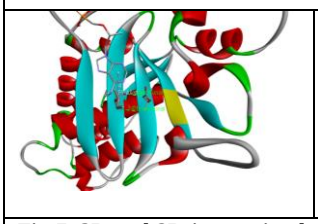

**Fig 6. 3D and 2D interaction between GP24 modelled refined protein with PubChem ID 37542**

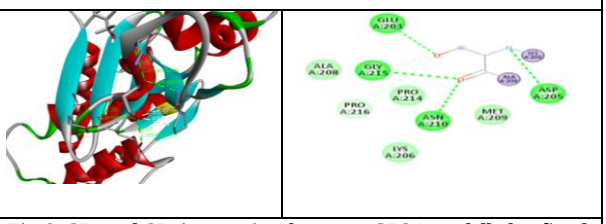

**Fig 7. 3D and 2D interaction between GP24 modelled refined protein with PubChem ID 64987**

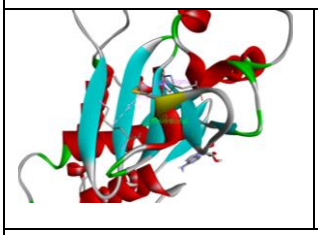

**Fig 8. 3D and 2D interaction between GP24 modelled refined protein with PubChem ID 91457**

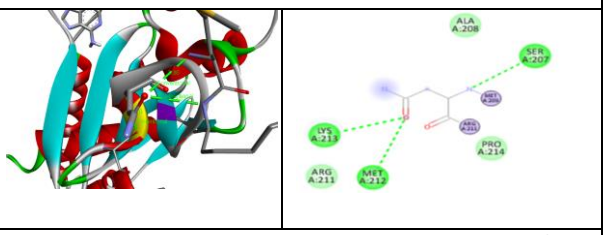

**Fig 9. 3D and 2D interaction between GP24 modelled refined protein with PubChem ID 96368**

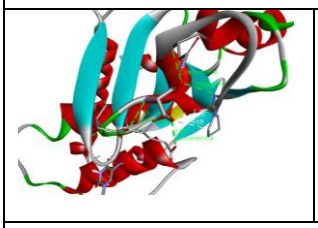

**Fig 10. 3D and 2D interaction between GP24 modelled refined protein with PubChem ID 102198**

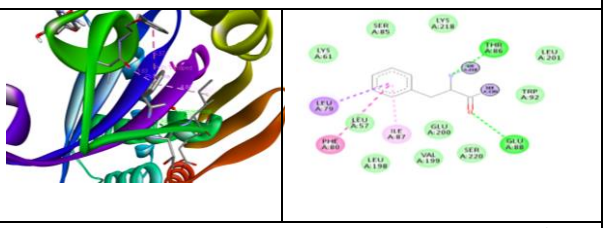

**Fig 11. 3D and 2D interaction between GP24 modelled refined protein with PubChem ID 254616**

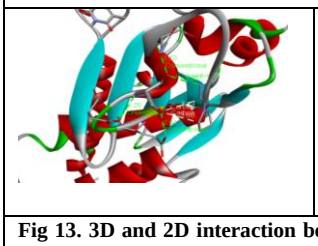

**Fig 12. 3D and 2D interaction between GP24 modelled refined protein with PubChem ID 256623**

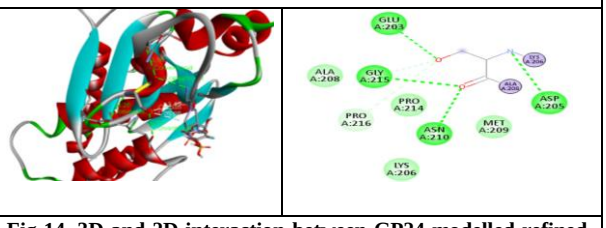

**Fig 13. 3D and 2D interaction between GP24 modelled refined protein with PubChem ID 374108**

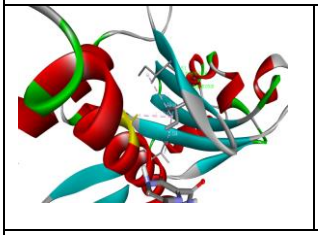

**Fig 14. 3D and 2D interaction between GP24 modelled refined protein with PubChem ID 416724**

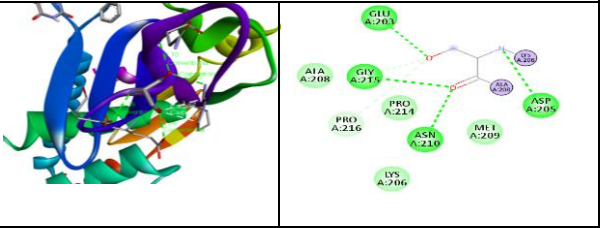

**Fig 15. 3D and 2D interaction between GP24 modelled refined protein with PubChem ID 492405**



**Fig 16. 3D and 2D interaction between GP24 modelled refined protein with PubChem ID 3851453**

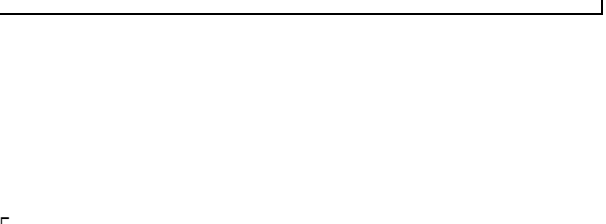

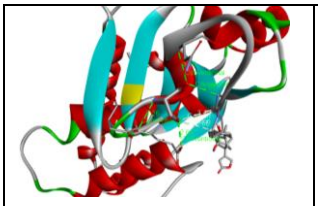

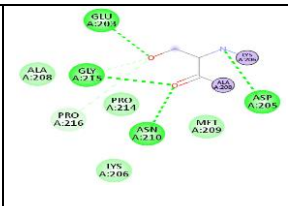

**Fig 17. 3D and 2D interaction between GP24 modelled refined protein with PubChem ID 4369270**

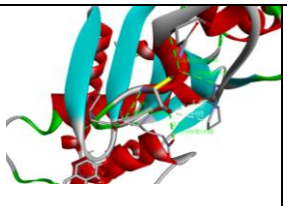

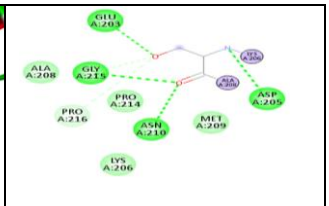

**Fig 18. 3D and 2D interaction between GP24 modelled refined protein with PubChem ID 5284371**

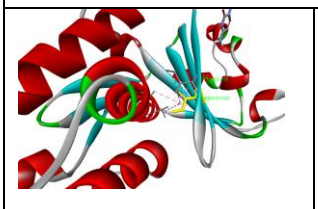

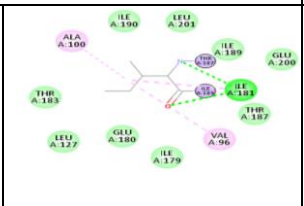

**Fig 19. 3D and 2D interaction between GP24 modelled refined protein with PubChem ID5351180**

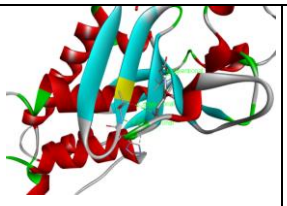

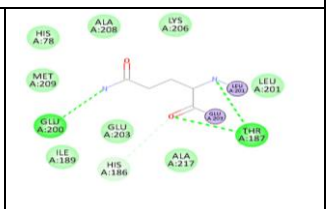

**Fig 20. 3D and 2D interaction between GP24 modelled refined protein with PubChem ID 44149862**

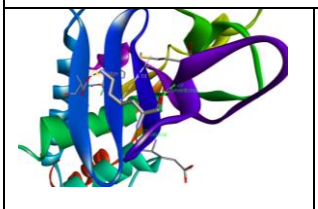

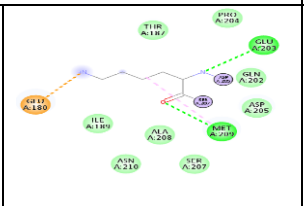

**Fig 21. 3D and 2D interaction between GP24 modelled refined protein with PubChem ID 44357643**

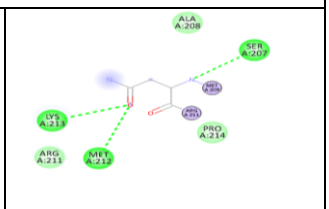

**Fig 22. 3D and 2D interaction between GP24 modelled refined protein with PubChem ID 54678599**

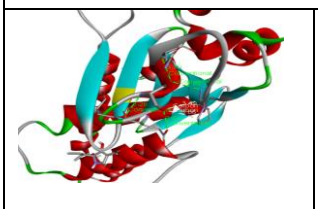

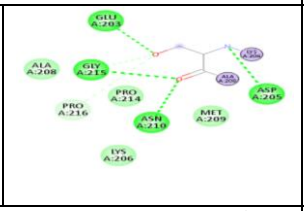

**Fig 23. 3D and 2D interaction between GP24 modelled refined protein with PubChem ID 54737266**

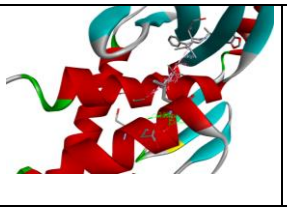

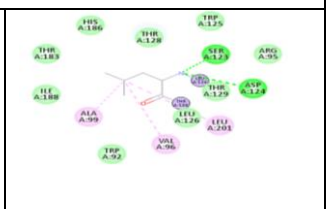

**Fig 24. 3D and 2D interaction between GP24 modelled refined protein with PubChem ID 45038223**

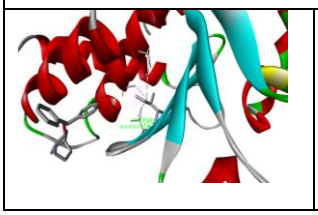

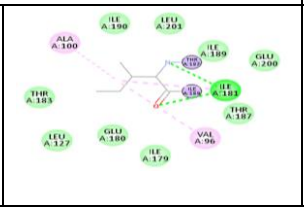

**Fig 25. 3D and 2D interaction between GP24 modelled refined protein with PubChem ID Benztropine**

Further MD simulation study was performed by using WebGro tools. Fully solvated molecular dynamics simulations are carried out by WebGro using the GROMACS simulation software (Fig 26-33). Users only need to input their protein file, which should end in.pdb, and WebGro will handle simulation and trajectory analysis. In light of existing research pertaining to GROMACS simulation, default values have been specified for the parameters in the submission page. The real motions of atoms and molecules are examined using a computer simulation method known as molecular dynamics (MD) (Roe et al., 2013). For a predetermined amount of time, the atoms and molecules are allowed to interact, providing insight into the system's dynamic "evolution." The features of such complex systems cannot be determined analytically since molecular systems often contain a large number of particles; MD simulation gets around this issue by employing numerical techniques. Long MD simulations, on the other hand, are theoretically unsound, leading to cumulative mistakes in numerical integration that can be reduced but not totally avoided with

the right choice of techniques and settings. It is possible to compare the outcomes of MD simulations to experiments that quantify molecular dynamics, one of which being NMR spectroscopy (Rothman et al., 2008). Even though the approach has historically had mixed results in this field, MD-derived structure predictions can be verified by community-wide studies in Critical Assessment of protein Structure Prediction (CASP) (Roe et al., 2013; Rothman et al., 2008). The RMSD, RMSF, and Rg values from the 50 ns molecular dynamics simulation results demonstrated that the suggested molecule was well equilibrated and, consequently, stable in the protein-ligand complex. This compound's (CID 3851453) significant binding affinities to the receptor cavity were consistent with the findings of the docking studies.

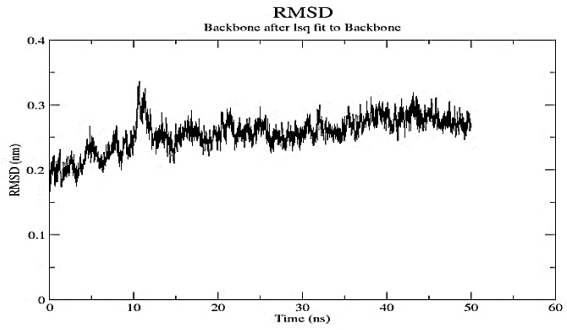


**Fig 26. RMSD Plot for READYMODELLEDPROTEIN_Structure2D_CID_3851453_out_1.-7.4.complex**

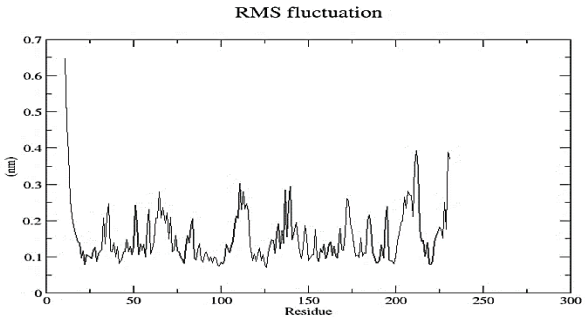


**Fig 27. RMSF Plot for READYMODELLEDPROTEIN_Structure2D_CID_3851453_out_1.-7.4.complex.**

The below plot (Fig 26) showed that the RMSD evolution of GP24 modelled refined protein. All protein frames were first aligned on the reference frame backbone and then the RMSD was calculated based on the atom selection. It gives insights into the protein's structural conformation throughout the simulation. Here found simulation had equilibriated and protein was having stable conformation during the simulation. RMSF is useful for characterizing local changes along the GP24 modelled refined protein chain (Fig 27).

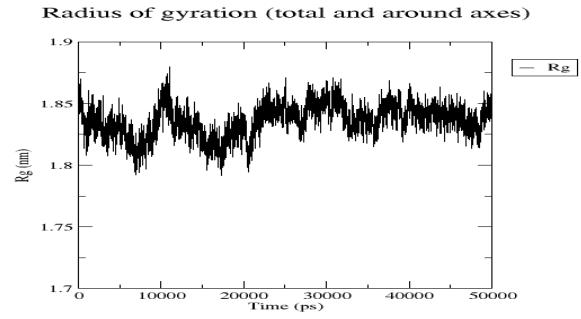


**Fig 28. Rg Plot for READYMODELLEDPROTEIN_Structure2D_CID_3851453_out_1.-7.4.complex.**

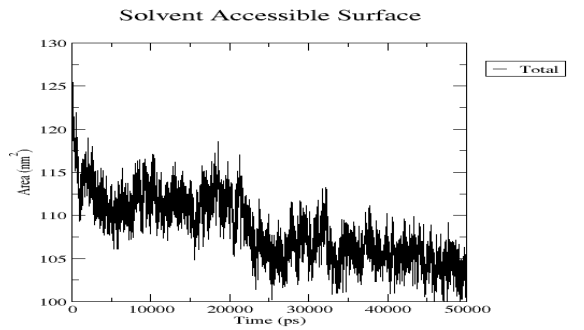


**Fig 29. SASA (total) Plot for READYMODELLEDPROTEIN_Structure2D_CID_3851453_out_1.-7.4.complex.**

Fig. 28 indicates Radius of gyration (Rg) which computes the radius of gyration (structural compactness) of GP24 modelled refined protein and the radii of gyration about the x-, y- and z-axes, plotted as a function of time. Fig. 29 is called as Solvent-accessible surface area (SASA) plot. It is considered as an approximate surface area of GP24 modelled refined protein that is accessible to a solvent with respect to simulation time. Fig. 30 indicates H bonds plot for GP24 modelled refined protein which is useful for interaction with ligand molecule.

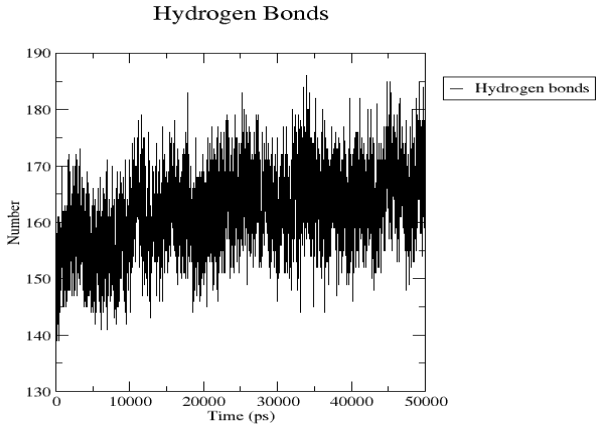


**Fig 30. H BONDS Plot for READYMODELLEDPROTEIN_Structure2D_CID_3851453_out_1.-7.4.complex**

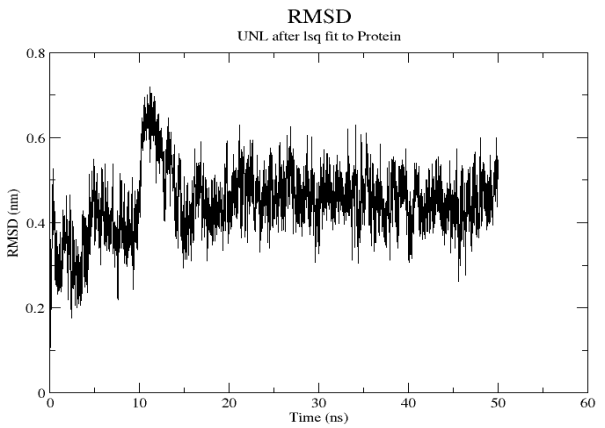


**Fig 31. Ligand RMSD Plot for READYMODELLEDPROTEIN_Structure2D_CID_3851453_out_1.-7.4.complex**

Ligand (CID 3851453) RMSD indicates how stable the ligand was with respect to the protein and its binding pocket (Fig. 31). This is also called as "LIG fit Prot". It predicts that the RMSD of a ligand when the protein-ligand complex is first aligned on the protein backbone of the reference and then the RMSD of the ligand heavy atoms was measured. Fig. 32 indicates stable H bonds formed between protein and ligand selected, whereas area per residue over the trajectory indictes by Fig 33.

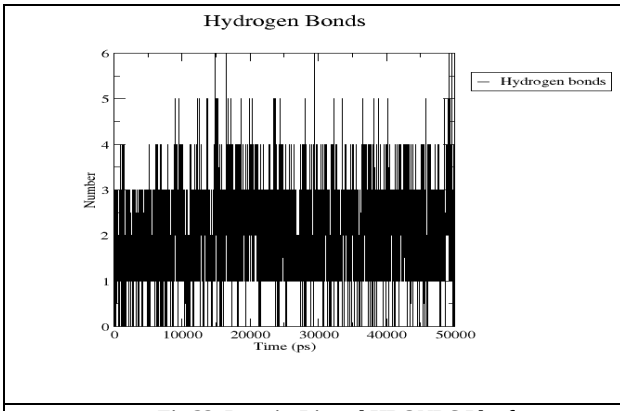


**Fig 32. Protein-Ligand HBONDS Plot for READYMODELLEDPROTEIN_Structure2D_CID_3851453_out_1.-7.4.complex**

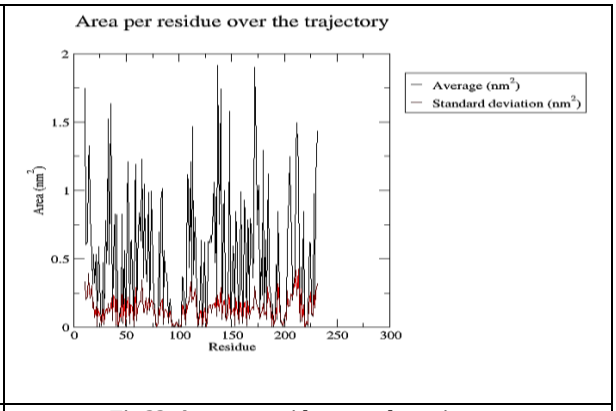


**Fig 33. Area per residue over the trajectory**

## Conclusion

Ebola has the unfortunate distinction of having some of the highest case-fatality rates of any pathogens that is currently understood. Novel antivirals are urgently required to combat Ebola virus infections. One molecule with the potential to become an antiviral medication for EBOV (CID 3851453) was chosen after a virtual screening of significantly 20 chemicals against the GP24 modelled refined protein structure of Ebola. -7.4 Kcal/mol of binding energies was discovered. Along with ADMET, the physiological and bioactivity parameters were accurately anticipated. The RMSD, RMSF, and Rg values from the 50 ns molecular dynamics simulation results demonstrated that the hypothesized compound was well equilibrated as well as, consequently, stable in the protein-ligand complex. This chemical's (CID 3851453) significant binding affinities to the receptor cavity were in line with the results of the docking studies. Furthermore, it is anticipated that the discovered inhibitor (CID 3851453) will make a better starting point for additional experimental research in the search for antiviral drugs.

## Conflict of Interest

The author hereby declares no conflict of interest.

## Consent for publication

The author declares that the work has consent for publication.

## Funding support

The author declares that they have no funding support for this study.

## References

Anders, E., Koch, R., & Freunscht, P. (1993). Optimization and application of lithium parameters for PM3. Journal of computational chemistry, 14(11), 1301-1312.

Antal Jr, M. J., Leesomboon, T., Mok, W. S., & Richards, G. N. (1991). Mechanism of formation of 2-furaldehyde from D-xylose. Carbohydrate Research, 217, 71-85.

Arooj, M., Sakkiah, S., Kim, S., Arulalapperumal, V., & Lee, K. W. (2013). A combination of receptor-based pharmacophore modeling & QM techniques for identification of human chymase inhibitors. PLoS One, 8(4), e63030.

Azam, S. S., & Abbasi, S. W. (2013). Molecular docking studies for the identification of novel melatoninergic inhibitors for acetylserotonin-O-methyltransferase using different docking routines. Theoretical Biology and Medical Modelling, 10(1), 1-16.

Balimane, P. V., Chong, S., & Morrison, R. A. (2000). Current methodologies used for evaluation of intestinal permeability and absorption. Journal of pharmacological and toxicological methods, 44(1), 301-312.

Beaulieu, D., & Ohemeng, K. A. (1999). Patents on bacterial tRNA synthetase inhibitors: January 1996 to March 1999. Expert Opinion on Therapeutic Patents, 9(8), 1021-1028.

Beeching, N. J., Fenech, M., & Houlihan, C. F. (2014). Ebola virus disease. BMJ 349: g7348.

Benet, L. Z., & Hoener, B. A. (2002). Changes in plasma protein binding have little clinical relevance. Clinical Pharmacology & Therapeutics, 71(3), 115-121.

Bissantz, C., Folkers, G., & Rognan, D. (2000). Protein-based virtual screening of chemical databases. 1. Evaluation of different docking/scoring combinations. Journal of medicinal chemistry, 43(25), 4759-4767.

Braga, E. J., Corpe, B. T., Marinho, M. M., & Marinho, E. S. (2016). Molecular electrostatic potential surface, HOMO–LUMO, and computational analysis of synthetic drug Rilpivirine. Int. J. Sci. Eng. Res, 7(7), 315-319.

Brehm, M. A., Bortell, R., Verma, M., Shultz, L. D., & Greiner, D. L. (2016). Humanized mice in translational immunology. Translational immunology: mechanisms and pharmacological approaches, 285-326.

Castillo-Garit, J. A., Marrero-Ponce, Y., Torrens, F., & García-Domenech, R. (2008). Estimation of ADME properties in drug discovery: predicting Caco-2 cell permeability using atom-based stochastic and non-stochastic linear indices. Journal of pharmaceutical sciences, 97(5), 1946-1976.

De Oliveira, A. M. (2018). Introdução à modelagem Molecular para Química, Engenharia e Biomédicas: fundamentos e exercícios. Appris Editora e Livraria Eireli-ME.

Desai, C. (2016). Meyler's side effects of drugs: The international encyclopedia of adverse drug reactions and interactions. Indian Journal of Pharmacology, 48(2), 224.

Dezani, T. M., Dezani, A. B., da Silva Junior, J. B., & dos Reis Serra, C. H. (2016). Single-Pass Intestinal Perfusion (SPIP) and prediction of fraction absorbed and permeability in humans: A study with antiretroviral drugs. European Journal of Pharmaceutics and Biopharmaceutics, 104, 131-139.

Feldmann, H., & Geisbert, T. W. (2011). Ebola haemorrhagic fever. The Lancet, 377(9768), 849-862.

Gasteiger, J., & Marsili, M. (1980). Iterative partial equalization of orbital electronegativity-a rapid access to atomic charges. Tetrahedron, 36(22), 3219-3228.

Irvine, J. D., Takahashi, L., Lockhart, K., Cheong, J., Tolan, J. W., Selick, H. E., & Grove, J. R. (1999). MDCK (Madin–Darby canine kidney) cells: a tool for membrane permeability screening. Journal of pharmaceutical sciences, 88(1), 28-33.

Khabbaz, R., Bell, B. P., Schuchat, A., Ostroff, S. M., Moseley, R., Levitt, A., & Hughes, J. M. (2015). Emerging and reemerging infectious disease threats. Mandell, Douglas, and Bennett's principles and practice of infectious diseases, 158.

Koes, D. R. (2018). The Pharmit backend: A computer systems approach to enabling interactive online drug discovery. IBM journal of research and development, 62(6), 3-1.

La Regina, G., Gatti, V., Piscitelli, F., & Silvestri, R. (2011). Open vessel and cooling while heating microwave-assisted synthesis of pyridinyl N-aryl hydrazones. ACS combinatorial science, 13(1), 2-6.

Lee, S. K., Lee, I. H., Kim, H. J., Chang, G. S., Chung, J. E., & No, K. T. (2003). The PreADME Approach: Web-based program for rapid prediction of physico-chemical, drug absorption and drug-like properties. EuroQSAR 2002 Designing Drugs and Crop Protectants: processes, problems and solutions, 2003, 418-420.

Loprinzi, C. L., Barton, D. L., & Qin, R. (2011). Nonestrogenic management of hot flashes. Journal of Clinical Oncology, 29(29), 3842-3846.

Ma, X. L., Chen, C., & Yang, J. (2005). Predictive model of blood-brain barrier penetration of organic compounds. Acta Pharmacologica Sinica, 26(4), 500-512.

Mali, S. N., & Chaudhari, H. K. (2019). Molecular modelling studies on adamantane-based Ebola virus GP-1 inhibitors using docking, pharmacophore and 3D-QSAR. SAR and QSAR in Environmental Research, 30(3), 161-180.

Morris, G. M., Goodsell, D. S., Halliday, R. S., Huey, R., Hart, W. E., Belew, R. K., & Olson, A. J. (1998). Automated docking using a Lamarckian genetic algorithm and an empirical binding free energy function. Journal of computational chemistry, 19(14), 1639-1662.

Morris, G. M., Huey, R., Lindstrom, W., Sanner, M. F., Belew, R. K., Goodsell, D. S., & Olson, A. J. (2009). AutoDock4 and AutoDockTools4: Automated docking with selective receptor flexibility. Journal of computational chemistry, 30(16), 2785-2791.

Mukund, V., Behera, S. K., Alam, A., & Nagaraju, G. P. (2019). Molecular docking analysis of nuclear factor-κB and genistein interaction in the context of breast cancer. Bioinformation, 15(1), 11.

Nimlos, M. R., Qian, X., Davis, M., Himmel, M. E., & Johnson, D. K. (2006). Energetics of xylose decomposition as determined using quantum mechanics modeling. The Journal of Physical Chemistry A, 110(42), 11824-11838.

Oso, B. J., Adeoye, A. O., & Olaoye, I. F. (2020). Pharmacoinformatics and hypothetical studies on allicin, curcumin, and gingerol as potential candidates against COVID-19-associated proteases. Journal of Biomolecular Structure and Dynamics, 1-12.

Ostroff, D., McDade, J., LeDuc, J., & Hughes, J. M. (2005). Emerging and re-emerging infectious disease threats. Principles and practice of infectious disease. Philadelphia, Elsevier Churchill Livingstone, 173-192.

Ramalingam, S., Babu, P. D. S., Periandy, S., & Fereyduni, E. (2011). Vibrational investigation, molecular orbital studies and molecular electrostatic potential map analysis on 3-chlorobenzoic acid using hybrid computational calculations. Spectrochimica Acta Part A: Molecular and Biomolecular Spectroscopy, 84(1), 210-220.

Roe, D. R., & Cheatham III, T. E. (2013). PTRAJ and CPPTRAJ: software for processing and analysis of molecular dynamics trajectory data. Journal of chemical theory and computation, 9(7), 3084-3095.

Rothman, R. B., Baumann, M. H., Prisinzano, T. E., & Newman, A. H. (2008). Dopamine transport inhibitors based on GBR12909 and benztropine as potential medications to treat cocaine addiction. Biochemical pharmacology, 75(1), 2-16.

Rougeron, V., Feldmann, H., Grard, G., Becker, S., & Leroy, E. M. (2015). Ebola and Marburg haemorrhagic fever. Journal of Clinical Virology, 64, 111-119.

Sarkar, D. (2021). Molecular Docking study to Identify Potent Fungal Metabolites as Inhibitors against SARS-CoV-2 Main Protease Enzyme. Int J Pharm Sci.12(2), b78-85 http://dx.doi.org/10.22376/ijpbs.2021.12.2.b78-85

Sarkar, D. (2022). In-silico research to screen various phytochemicals as potential therapeutics againstbeta glucan synthase enzyme from black fungus endangering COVID patients in India. Intern. J. Zool. Invest. 8(1): 320-337 https://doi.org/10.33745/ijzi.2022.v08i01.035

Sarkar, D., Ganguly, A. (2022). Molecular Docking Studies with Garlic Phytochemical Constituents To Inhibit The Human EGFR Protein For Lung Cancer Therapy. Int J Pharm Sci.13(2), B1-14 http://dx.doi.org/10.22376/Ijpbs.2022.13.2.b1-14

Sarkar, D., Maiti, A. K. (2023). Virtual Screening and Molecular Docking Studies with Organosulfur and Flavonoid Compounds of Garlic Targeting

the Estrogen Receptor Protein for the Therapy of Breast Cancer. Volume 13, Issue 1, 2023, 49 https://doi.org/10.33263/BRIAC 131.049

Sarkar, D., Maiti, A.K., Rawaf, A., Babu, J. (2022). In silico Approach to Identify Potent Bioactive Compounds as Inhibitors against the Enoyl-acyl Carrier Protein (acp) Reductase Enzyme of Mycobacterium tuberculosis. Volume 12, Issue 5, 7023 – 7039 https://doi.org/10.33263/BRIAC 125.70237039

Wadapurkar, R. M., Shilpa, M. D., Katti, A. K. S., & Sulochana, M. B. (2018). In silico drug design for Staphylococcus aureus and development of host-pathogen interaction network. Informatics in Medicine Unlocked, 10, 58-70.

Wenthur, C. J., Gentry, P. R., Mathews, T. P., & Lindsley, C. W. (2014). Drugs for allosteric sites on receptors. Annual review of pharmacology and toxicology, 54, 165-184.

**How to cite this article**

Sarkar, D. and Ahamad, Sk. M. (2022). Finding antagonist for the VP24 protein of the Ebola virus to treat infections using molecular docking and molecular dynamics studies. *Science Archives,* Vol. *3*(4), 289-300 https://doi.org/10.47587/SA.2022.3408